energies

MDPI

Article

Study on Optimization of Copper to Aluminum for Locomotive Finned Tube Radiator

Ying Guan, Hongjiang Cui * and Jiyou Fei

School of Locomotive and Rolling Stock Engineering, Dalian Jiaotong University, Dalian 116028, China
* Correspondence: chj@djtu.edu.cn

Abstract: The influence of the improvement of the finned tube radiator unit structure on the fluid flow and heat transfer effect of the locomotive was studied. A saw-toothed fin structure with aluminum instead of copper was proposed to keep the position and size of the flat copper hot water pipe unchanged. CFD simulation analysis was carried out by ICEPAK17.0, under the conditions of an ambient temperature of 24.6 °C, atmospheric pressure of 85,040 Pa and air density ρ = 0.94 kg/m^3, to compare the changes of velocity field, temperature field, turbulence field and field synergy angle. The sawtooth structure of the new heat sink increases the turbulence effect of the fluid, reduces the thickness of the outer boundary layer of the water pipe, and strengthens the heat transfer effect of the radiator. Finally, the baffle height, wing window width and sawtooth angle of the sawtooth structure were selected, and the heat transfer coefficient and pressure under three conditions of low, medium and high were used as indexes to analyze the influence of each parameter on the performance of the radiator. The results show that the heat dissipation effect of the serrated aluminum sheet is higher than that of the copper sheet, the heat transfer coefficient is increased by about 1.3%, the average pressure is reduced, the turbulence performance is improved, the synergy angle is reduced by about 2.3°, and the new radiator has better performance. The fin factor has the greatest influence on the heat transfer coefficient and the least influence on the pressure. When the baffle is about 0.15 mm high, the heat transfer coefficient is the largest, and the height change has the highest effect on the pressure. The included Angle factor has the least influence on the heat transfer effect, and the influence on the pressure is higher. By changing the fin window structure, the thermal performance of the finned tube radiator can be improved.

Keywords: finned tube radiator; sawtooth fin window; CFD; field synergy; optimization

Citation: Guan, Y.; Cui, H.; Fei, J. Study on Optimization of Copper to Aluminum for Locomotive Finned Tube Radiator. *Energies* **2023**, *16*, 2130. https://doi.org/10.3390/en16052130

Academic Editors: Feng Cao, Xiang Yin and Yulong Song

Received: 15 December 2022
Revised: 5 February 2023
Accepted: 16 February 2023
Published: 22 February 2023

1. Introduction

The cooling system of rail vehicles is mainly composed of radiators, intercoolers, heat exchangers, water pumps, fans and other components, which directly affect the structural layout of the locomotive, various technical and economic indicators and operational reliability [1–6]. Changing the main structure of the radiator from copper material to aluminum material can achieve the purpose of making it lightweight and economical. However, since the thermal conductivity of copper is better than aluminum, the structure of the radiator needs to be improved.

At present, in the related research on the fin radiator, domestic and foreign scholars have carried out extensive research on the influence of fin structure on heat transfer performance. Aris et al. [7] studied the influence of the delta wing structure and its placement on the heat transfer effect. Gu et al. [8–12] studied the effect of fin side length and fin spacing on the heat dissipation of the radiator, and found that the fin spacing was 3 mm and the fin side length was 90 mm when the radiator had the best performance. Zullo Federico et al. [13–15] studied the influence of structural parameters such as fin height, thickness, pitch and window fin height on the performance of the radiator. Wang [16] compared the influence of u-type and l-type heat exchange tube insertion methods on the

thermal performance of the radiator. Le et al. [17,18] studied the effect of heat transfer tube spacing, fin length and number on the heat transfer of heat pipes. Dawid Taler et al. [19–23] obtained the correlation between heat transfer and friction coefficients by the multiple regression method, and established a mathematical model for evaluating the performance of the radiator. Bisri et al. [24–28] analyzed the effect of different fin spacings on the heat transfer effect of the radiator and fuel heating. Wang Baozhong [29–34] optimized the airfoil of the flat water tube structure and studied the influence of structural parameters on the performance of the radiator. Maisuria et al. [35–39] studied the influence of the addition of different component fluids and nanoparticles on the net heat transfer rate of the radiator. Jin et al. [40–44] discussed the pressure drop and heat transfer effects of the inclined fin tube bundles with different angles, and obtained the best effect at 45°, and the mass flow and heat transfer growth rates reached 12.81% and 8.96%, respectively. Promvonge and Skullong [45] compared the effects of perforated delta wings and elliptical wings, as well as solid triangle and ellipse structures, on the performance of heat exchangers, and found that the thermal performance enhancement factor of the wing structure was 5–8% higher than that of the solid structure, and the thermal performance enhancement factor of the delta wing was the largest when the perforation size was 0.417 in the low Re condition, which was about 2.17.

In summary, current domestic and foreign research mainly focuses on the heat exchange tube form, arrangement, fin parameters and spacing, etc. There is less research on the heat dissipation of fin materials and fin window structure. The fin window structure can promote the air mixing in different flow channels, affect the boundary layer of the hot water pipe wall, and enhance the disturbance of the circulating air, thereby improving the heat transfer effect of the radiator. Therefore, in improving the heat transfer of the radiator, the optimization of the fin window structure is very important. On the basis of referring to domestic and foreign research, the radiator material is changed from copper to aluminum, keeping the position of the hot water pipe structure unchanged, a new type of heat sink with fin window structure is proposed, and the influence of fin window parameters on the performance of the radiator is discussed.

2. CFD Simulation and Test Verification

2.1. Model Establishment

A certain type of locomotive finned tube radiator is taken as the research object. Figure 1 is a physical model of one of the radiators. Figure 2 is a schematic diagram of the main structure of the radiator. The size structure is shown in Table 1.

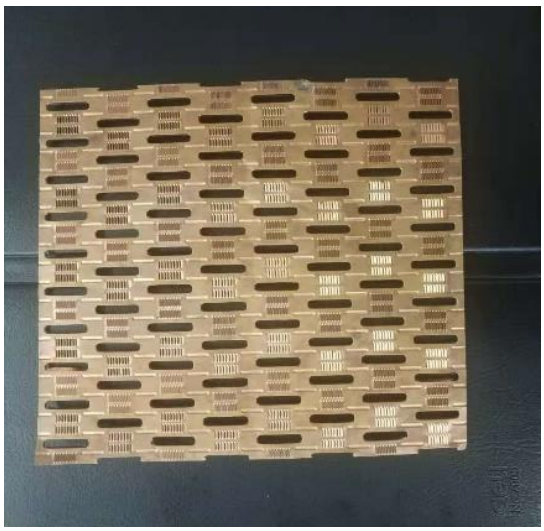

Figure 1. Diagram of the radiator fin.

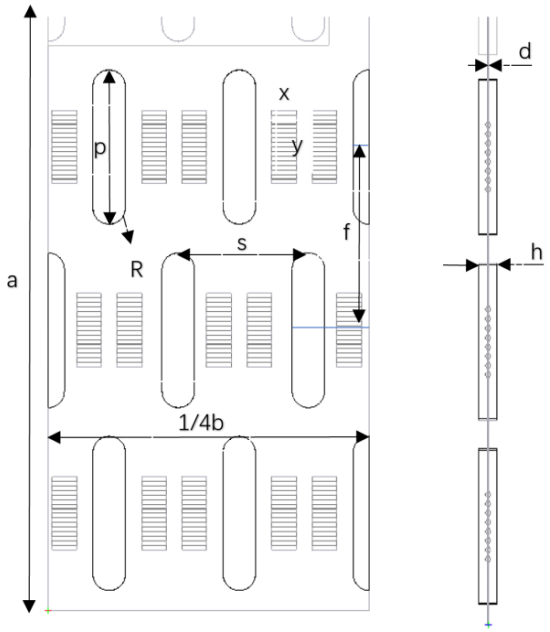

Figure 2. Structure diagram of the radiator fin.

Table 1. Structure parameters of the radiator fin.

Parameters	Numerical Value
Heat sink height a (mm)	180
Heat sink width b (mm)	160
Heat sink pitch h (mm)	2.33
Heat sink thickness d (mm)	0.16
Longitudinal spacing of hot water pipes f (mm)	22.5
Horizontal spacing of hot water pipes s (mm)	16
Arc radius of hot water pipe R (mm)	2
Hot water pipe height p (mm)	19
Blinds height y (mm)	3
Width of blinds x (mm)	9

The complete radiator has a huge structure, symmetry and a large number of repetitive structures. Under the premise of ensuring the calculation accuracy and results, the model is simplified in order to reduce the calculation time. The representative unit structure of the radiator is intercepted, the height is unchanged and the width is 1/4. In order to develop the air movement fully, the extension area of the entrance and exit is established. References [46–49] establish the calculation model of the radiator unit structure. Three monitoring points are set evenly in the middle of the river basin on one side, denoted by a, b, and c, as shown in Figure 3.

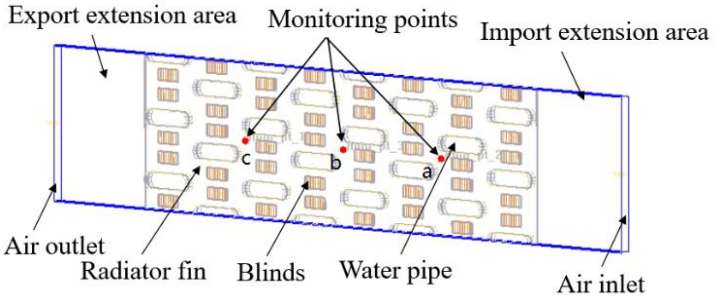

Figure 3. Structural calculation model of the radiator.

2.2. Boundary Conditions and Governing Equations

1. By default, the internal fluid movement in the calculation model is turbulent, and the Boussinesq approximation and standard model are used to perform simulation calculations by solving three-dimensional continuity equations, energy equations and momentum equations. 2. It is assumed that the fins are isotropic, and the material of the fins and the water pipe is copper. 3. Set the air and water pipes as speed inlets and at constant temperature, and the inlet fluid flow rate is evenly distributed. Since the water pipe section is cut short, the influence of gravity is ignored. 4. The physical properties of air and water do not change with temperature changes. 5. The spacing of each runner is even, and the ventilation and heat exchange conditions are the same. 6. Ignore the influence of fluid viscosity dissipation and shutter thickness on fluid movement. 7. According to the test conditions, it is determined that the ambient temperature is 24.6 °C, the atmospheric pressure is 85,040 Pa, and the air density, ρ = 0.94 kg/m^3. 8. Adopting pressure–velocity coupling with SIMPLE, the residual error value is 1×10^{-3}. The number of iterations is 600. References [50–54] governing equations, the Boussinesq model and standard model transportation equations are shown below.

Continuity equation

$$\frac{\partial \rho}{\partial t} + \nabla \cdot (\rho \vec{v}) = 0 \tag{1}$$

Energy equation

$$\frac{\partial}{\partial t}(\rho h) + \nabla \cdot (\rho h \vec{v}) = \nabla \cdot [(k + k_t)\nabla T] + S_h \tag{2}$$

$$h = \int_{T_{ref}}^{T} c_p dT_t \tag{3}$$

$$k_t = c_p \mu_t / Pr_t \tag{4}$$

Momentum equation

$$\frac{\partial}{\partial t}(\rho \vec{v}) + \nabla \cdot (\rho \vec{v}\vec{v}) = -\nabla p + \nabla \cdot (\bar{\bar{\tau}}) + \rho \vec{g} + \vec{F} \tag{5}$$

$$\bar{\bar{\tau}} = \mu \left[(\nabla \vec{v} + \nabla \vec{v}^T) - \frac{2}{3} \nabla \cdot \vec{v} I \right] \tag{6}$$

where p is static pressure, $\bar{\bar{\tau}}$ is the stress tensor, $\rho \vec{g}$ is the volume force of gravity, $\vec{F}$ is the force caused by resistance or other reasons, h is the sensible enthalpy, k is the heat transfer coefficient of the fluid, k_t is the heat transfer coefficient caused by turbulent motion, S_h is the heat source term of the defined volumetric heat source, μ is the hydrodynamic viscosity, and I is the unit tensor.

Boussinesq model

$$(\rho - \rho_0) g \approx -\rho_0 \beta (T - T_0) g \tag{7}$$

In the formula, ρ_0 is the fluid density constant, T_0 is the working temperature, and β is the thermal expansion coefficient.

Standard $k - \varepsilon$ model transportation equation

$$\frac{\partial}{\partial t}(\rho k) + \frac{\partial}{\partial x_i}(\rho k u_i) = \frac{\partial}{\partial x_i}\left[\left(\mu + \frac{\mu_t}{\sigma_k} \right) \frac{\partial k}{\partial x_i} \right] + G_k + G_b - \rho \varepsilon \tag{8}$$

$$\frac{\partial}{\partial t}(\rho \varepsilon) + \frac{\partial}{\partial x_i}(\rho \varepsilon u_i) \left[\left(\mu + \frac{\mu_t}{\sigma_\varepsilon} \right) \frac{\partial \varepsilon}{\partial x_i} \right] + C_{1\varepsilon} \frac{\varepsilon}{k} (G_k + C_{3\varepsilon} G_b) - C_{2\varepsilon} \rho \frac{\varepsilon^2}{k} \tag{9}$$

$$\mu_t = \rho C_\mu \frac{k^2}{\varepsilon} \tag{10}$$

In the formula, G_k represents the turbulent kinetic energy due to the average velocity gradient, G_b is the turbulent kinetic energy due to buoyancy, $C_{1\varepsilon}$, $C_{2\varepsilon}$, $C_{3\varepsilon}$ and C_μ are constants, and σ_k and σ_ε represent the Prandtl numbers of k and ε, respectively.

2.3. Meshing and Test Verification

The Mesher-HD grid is used for the entire calculation area, and a non-continuous grid area is established for the water pipe part through the discontinuous division technology. The grid independence is tested, and the heat transfer coefficient under the working condition of the air inlet velocity of 17.16 m/s is used as the evaluation index. The results of the discussion are shown in Figure 4, according to the cabinet size, at the max element size of 220,000, $V = 3.95 \times 22 \times 0.22$, at the max element size of 390,000, $V = 1.975 \times 11 \times 0.11$, and at the max element size of 1,060,000, $V = 1.975 \times 5.5 \times 0.11$. Finally, a division method with a grid number of approximately 390,000 is selected.

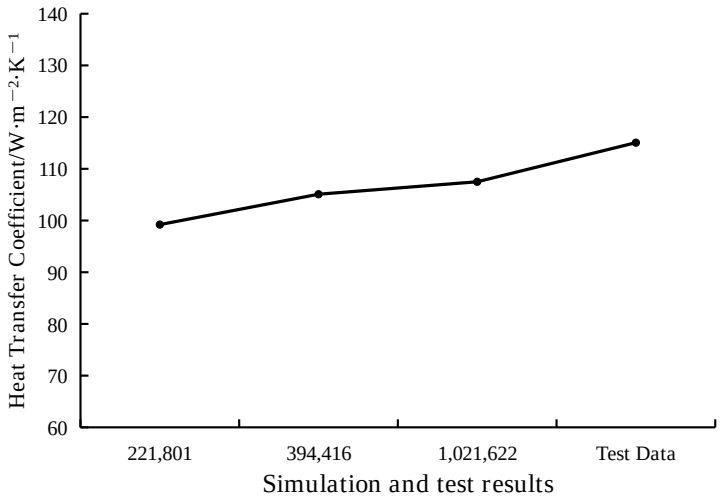

Figure 4. Discussion on grid dependence.

Using Icepak17.0, which adopts double precision, based on the pressure solver, the SIMPLE algorithm is adopted to improve the steady-state pressure speed coupling calculation. The test data were obtained at the Cooling Components Quality Supervision and Inspection Center of Lanzhou Jiaotong University in 2015. The data of each test condition are shown in Table 2. Figure 5 is a graph showing the comparison between the original data of the finned tube radiator test and the heat transfer coefficient of the simulation. The results show that the maximum deviation of the heat transfer coefficient is less than 10%, and the simulation results are consistent with the experimental data, and the experimental results can be predicted.

Table 2. Radiator test data.

Serial Number	Intake Air Temperature (°C)	Air Velocity (m/s)	Inlet Water Temperature (°C)	Water Velocity (m/s)	Heat Transfer Coefficient ($W \cdot m^{-2} \cdot K^{-1}$)
1	39.73	5.85	85.58	0.6	74.09
2	41.61	7.42	83.05	0.6	86.46
3	41.61	8.59	78.80	0.6	92.38
4	41.84	10.74	76.70	0.6	101.77
5	41.64	12.86	73.68	0.6	107.63
6	43.05	14.99	72.48	0.6	110.90
7	43.18	17.16	71.58	0.6	115.06

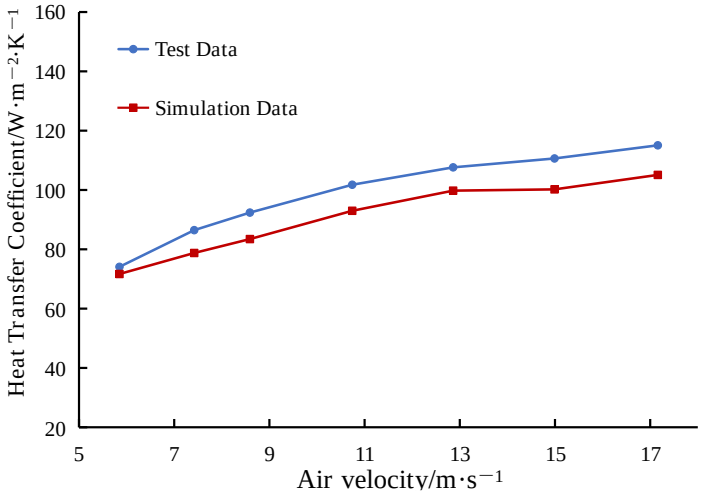

Figure 5. Comparison of simulation and test data.

3. Performance Analysis of Serrated Fin Window Radiator

Changing the radiator material from copper to aluminum can make the radiator lighter and more economical. In order to ensure that the performance of the radiator is not reduced, a serrated fin window structure is proposed to improve the radiator. Compared with the louver structure, serrated fin windows can reduce the thickness of the outer boundary layer of the water pipe and promote heat exchange, and the modified part of the radiator is only the fin window, which does not affect the original water pipe arrangement. Figure 6 shows the structure of the radiator unit of the sawtooth fin window. Equi-angle baffle structures are staggered on the edge of the fin window to increase air disturbance. The dimensions of the fin window structure are shown in Table 3.

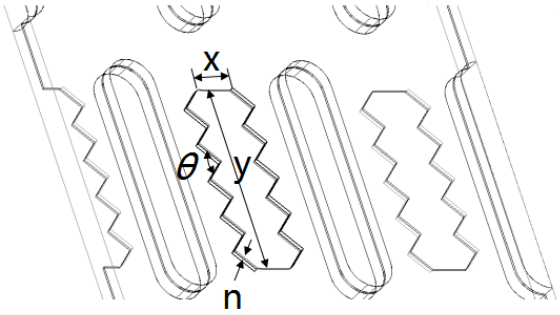

Figure 6. Structure diagram of the serrated fin window.

Table 3. Structural parameters of the serrated fin window.

Parameters	Numerical Value
Wing window width x (mm)	3
Wing window height y (mm)	15
Sawtooth-included angle θ(mm)	90
Baffle height n (mm)	0.3

The same simulation conditions are used for the numerical calculation of the sawtooth fin window radiator for each working condition, and the comparison with the original structure radiator is performed. Figure 7 shows the comparison of the temperature cloud diagrams of the two radiators on the plane where the monitoring point is located under the working condition of an air velocity of 17.16 m/s. It can be seen from the figure that after the cold air flows through the first row of hot water pipes, the gas temperature at

the leeward side of the water pipe has a significant increase in the improved model, the range of the higher gas temperature area becomes wider, and the airflow temperature on the long side of the water pipe rises, showing that the heat exchange between the cold air and the hot water pipe is more sufficient. This is because the serrated baffle increases the disturbance of the air flow direction and affects the thickness of the boundary layer outside the hot water pipe. The thickness of the boundary layer is reduced, the thermal resistance is reduced, the contact of cold air is more sufficient, and the heat exchange effect is improved.

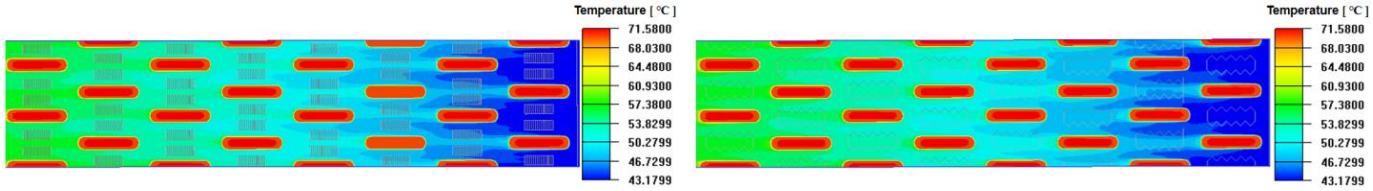

(**a**) (**b**)

Figure 7. Temperature cloud map in the basin before and after improvement; (**a**) original model; (**b**) improved model.

Figure 8 is the velocity cloud diagram under the same working condition. It can be seen from Figure 8 that the air circulation effect of the improved model is better, and the unevenness of the overall velocity distribution is alleviated. The air velocity of the hot water pipe decreases, and the low-speed area increases. The air velocity on the side adjacent to the sawtooth baffle increases significantly, and the range of the high-velocity area increases, which affects the leeward side of the hot water pipe, and reduces the range of the low-air velocity area on the leeward side. The circulation effect of cold air in the area is improved, and the maximum air velocity is about 35.75 m/s, which is about 6.87% lower than the original model. The change in the flow rate of the cold air can correspond to the temperature change phenomenon in Figure 7, reflecting the improvement of the air circulation and heat exchange effect of the improved structure.

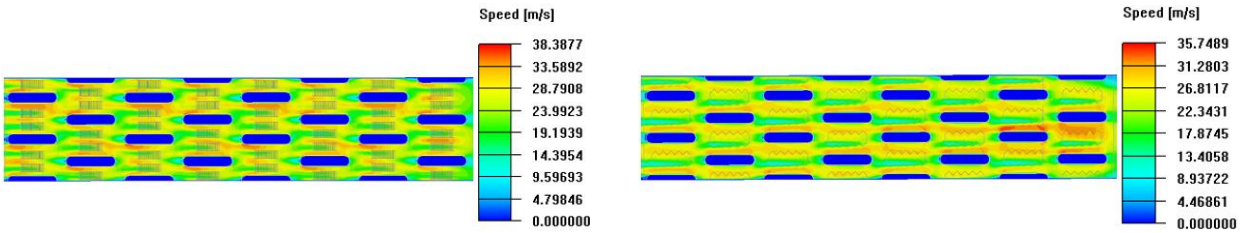

(**a**) (**b**)

Figure 8. Speed cloud map in the basin before and after improvement; (**a**) original model; (**b**) improved model.

According to the monitoring points set above, the average pressure inside the flow channel, turbulent flow energy, dissipation rate and synergy angle are measured, and the performance of the two radiators is compared with the heat transfer coefficient. The comparison result is shown in Figure 9. According to the literature [55–58], the field synergy relationship between the velocity vector and the temperature gradient vector in the flow channel is as follows.

$$u \cdot \nabla \overline{T} = |u| \cdot |\nabla T| \cos \beta \tag{11}$$

In the formula, β is the angle between the velocity vector and the temperature gradient vector (heat vector).

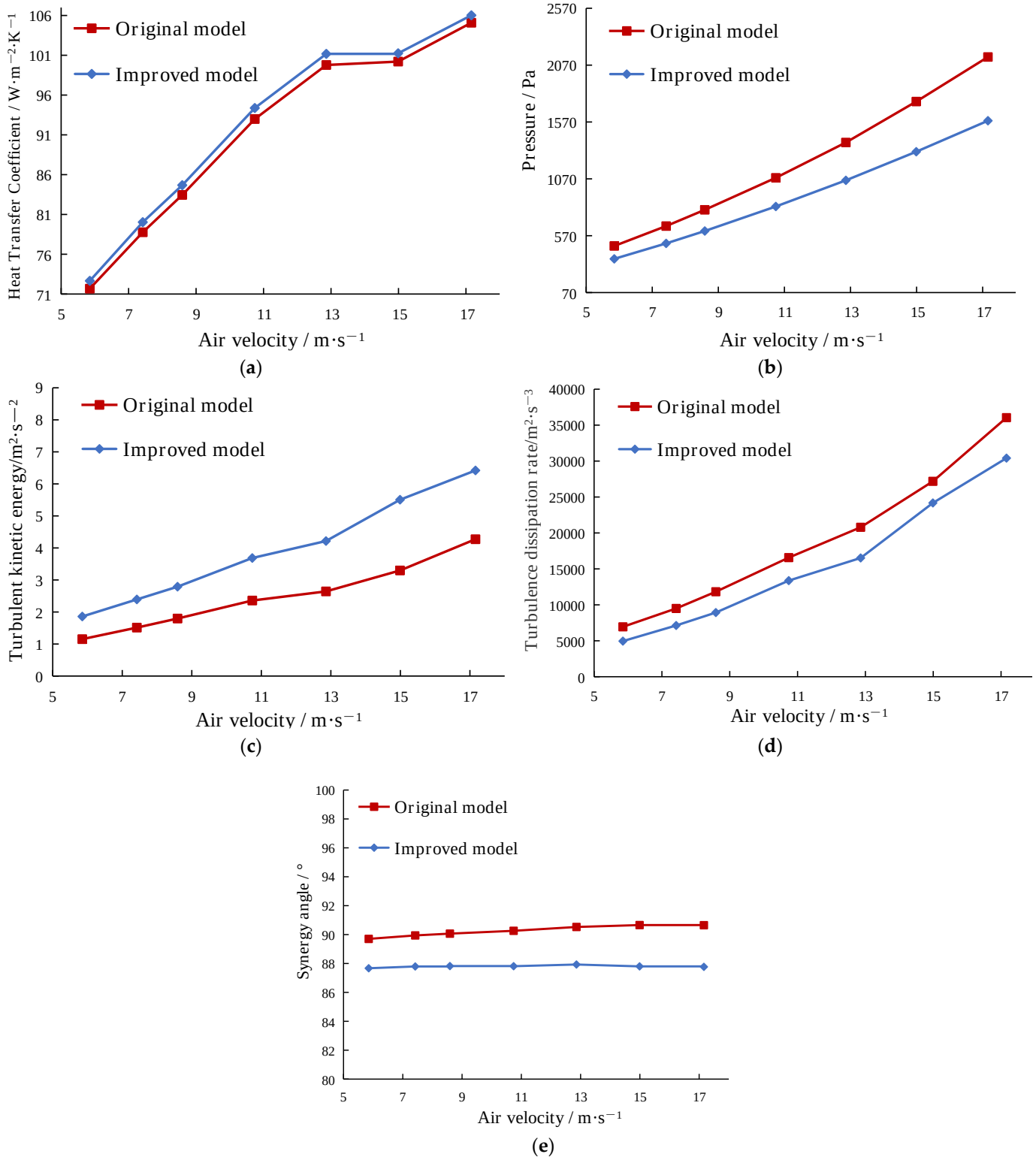

Figure 9. Comparison of performance before and after improvement; (**a**) heat transfer coefficient comparison; (**b**) pressure comparison; (**c**) turbulent kinetic energy comparison; (**d**) comparison of turbulence dissipation rate; (**e**) comparison of the law of synergy angle change.

It can be seen from Figure 9 that in the test conditions the improved heat transfer coefficient is greater than that of the original model, increasing by about 1.3%. Contrary to the change law of heat transfer coefficient, the pressure of the improved model is lower

than that of the original model, and the pressure difference increases with the increase of the air flow rate. Compared with the original structure, the average pressure in the flow rate range is reduced by about 24.59%. Comparing the turbulent kinetic energy of the two radiators, it can be seen that the turbulent kinetic energy of the improved model varies from k = 1.86 to 6.42, and the parameter of the original model varies from k = 1.15 to 4.27, and the turbulence energy increases by about 57.78% on average, indicating that the serrated fin window structure can significantly improve the turbulence performance of the air in the flow channel. Compared with Figure 9d, the turbulent dissipation rate of the improved structure is lower than that of the original structure, with an average reduction of about 18.13%, and the stability of turbulence under the serrated fin window is better. It can be seen from Figure 9e that, for a certain structure, the angle between the velocity vector and the temperature gradient vector is relatively determined, that is, the coordination angle is mainly related to the model structure, the synergy angle range of the original model fluctuates up and down by 90°, while the synergy angle of the improved model roughly fluctuates around 87.7, which is about 2.3° lower than the original model. It shows that the air flow of the sawtooth aluminum sheet is more synergistic with the heat propagation direction.

In summary, although the thermal conductivity of aluminum is lower than that of copper, the improved method of the zigzag fin window structure can make the aluminum radiator within the range of 5.85–17.16 m/s and have a higher heat dissipation effect, the turbulent flow can be significantly improved, the cold air cools the hot water pipe more fully, the pressure is reduced, and the serrated fin window structure is more reasonable in terms of the heat transfer angle.

4. Research on the Influence of Different Parameters

Through the analysis of the structure size of the sawtooth fin window, the influence of the height of the baffle, the width of the fin window and the angle of the sawtooth on the aluminum radiator of the new structure are considered separately, and the heat transfer coefficient and average pressure of the three working conditions of inlet wind speed of 5.85 m/s, 10.74 m/s and 17.16 m/s, respectively, are used as evaluation indicators. On the basis of the sawtooth fin window structure in Table 3, for each factor, the influence of four additional horizontal parameters on the performance of the radiator under low-speed, medium-speed and high-speed operating conditions is discussed. The relationship between the factors and levels is shown in Table 4, and the results are shown in Figures 10 and 11.

Table 4. Horizontal factor relationship table.

Level\Factor	A Baffle Height (mm)	B Wing Window Width (mm)	C Sawtooth-Included Angle (°)
1	0	1	60
2	0.15	2	75
3	0.3	3	90
4	0.45	4	105
5	0.6	5	120

From the influence of various factors on the heat transfer coefficient in Figure 10, it can be seen that, within the selected horizontal range, the height of the baffle and the width of the fin window have a greater influence on the heat transfer coefficient than the serrated angle. In the height of the baffle of 0–0.6 mm, the three air flow velocity working conditions are the same, and the heat transfer coefficient first increases, then decreases and then increases. At the height of the 0.15 mm baffle, the heat transfer coefficient is the highest, and the increase in the heat transfer coefficient is gentle, in the range of 0.3–0.6 mm. The three flow velocity conditions within the width of the 1–5 mm fin window have the same law, the heat transfer coefficient gradually decreases, and the range of change is the

largest. The heat transfer coefficient of the sawtooth-included angle changes smoothly from 60° to 120°, and the changing law is relatively complicated; the 120° heat transfer coefficient is the highest under low-speed conditions, and the 60° heat transfer coefficient is the highest under medium- and high-speed conditions.

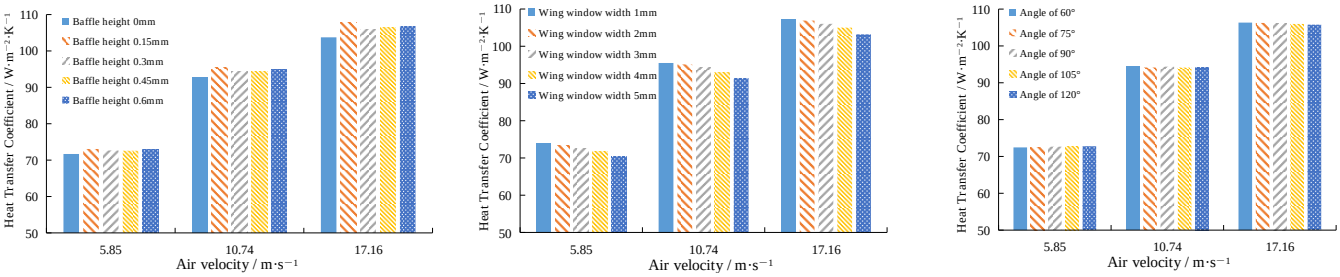

Figure 10. The influence of three factors on the heat transfer coefficient; (**a**) baffle factor; (**b**) wing window factor; (**c**) angle factor.

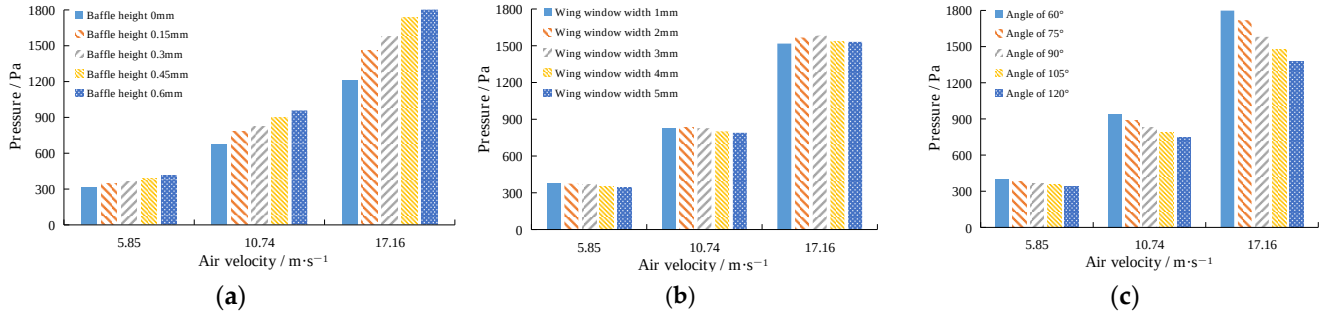

Figure 11. The influence of three factors on the pressure; (**a**) baffle factor; (**b**) wing window factor; (**c**) angle factor.

Comparing the influence of each factor level in Figure 11 on the pressure, it can be seen that the baffle height and the sawtooth-included angle have a greater influence on the pressure than the wing window factor. The first two factors have a more significant influence on the pressure as the air flow rate increases. The pressure of the plate height increases continuously, and the law is the same under the three working conditions in the horizontal range. The influence of the width of the fin window on the pressure under various working conditions is more complicated. The pressure change is small under low-speed conditions and the maximum pressure is when the fin window is 1 mm wide, under medium-speed conditions the maximum pressure is when the fin window width is 2 mm, and under high-speed conditions the maximum pressure is when the fin window width is 3 mm. The angle factor has the same law under the three working conditions. The pressure decreases continuously from 60° to 120°, and the pressure decrease is smaller than the baffle factor.

In summary, the effect on the heat transfer coefficient is fin window factor > baffle factor > included angle factor, and for the influence of average pressure, baffle factor > included angle factor > wing window factor. The heat transfer coefficient is the largest when the width of the fin window is 1 mm, which may be due to the larger fin volume and area under this size, which is beneficial to heat conduction and exchange, and has the least impact on pressure. When the baffle is 0.15 mm high, it can affect the air flow in the flow channel and increase the heat transfer coefficient, but further increase will hinder the flow and cause the pressure to rise sharply. The angle factor has the least influence on the heat transfer effect, and the increase of the angle reduces the heat transfer effect, significantly changes the air movement in the flow channel, and has a higher impact on the pressure.

5. Conclusions

Through the computational fluid dynamics analysis of the finned tube radiator unit structure of a certain locomotive, the simulation results are compared with the experimental data, and then a new fin window structure scheme of changing the heat sink from copper to aluminum is proposed. By comparing the performance of the two radiators, finally selecting the three factors of fin window baffle, width and included angle, and analyzing the law of the influence of each level on the performance of the radiator, the following conclusions are drawn.

(1) The test data are in good agreement with the simulation results, and the change trend is consistent, which proves the rationality of the simulation method in this paper and that it can be used to predict the actual situation.
(2) The heat transfer coefficient of the zigzag fin window aluminum heat sink is higher than that of the louver copper fin within the range of the test air flow rate, which is increased by about 1.3%, and the average pressure is reduced by about 24.59%, the turbulent flow energy is increased by about 57.78% on average, and the turbulent dissipation rate is decreased by about 18.13% on average, and, combined with the field synergy theory, the synergy angle is reduced by about 2.3°, and the performance of the new structure radiator is better.
(3) The fin window factor has the greatest influence on the heat transfer coefficient and the least influence on the pressure. The baffle factor has a higher influence on the heat transfer coefficient. The heat transfer coefficient is the largest when the height is 0.15 mm, and the height change has the highest influence on the pressure. The angle factor has the least influence on the heat transfer effect and has a higher influence on the pressure.

The findings from the current research offer a solution to improve the thermal performance of the finned tube radiator through changing the fin window structure. From the perspective of materials, manufacturing cost and reliability, the research on fin structure and thermal performance has need for further development in the future.

Author Contributions: Conceptualization, H.C.; methodology and software, Y.G.; validation, H.C. and Y.G.; investigation, data curation, J.F.; writing—original draft preparation, Y.G. and H.C. All authors have read and agreed to the published version of the manuscript.

Funding: This research was funded by the Science Researching Plans of Liaoning Provincial Education Department under Grant No. LJKZ0509 and No. LJKFZ20220203. The research was funded by Science and Technology Project of Liaoning Provincial Transportation Department under Grant No. 202242.

Data Availability Statement: Not applicable.

Acknowledgments: We would like to thank the Liaoning Provincial Department of Education and the Liaoning Provincial Department of Transportation for providing financial support for this research. Meanwhile, we would like to thank Dalian Jiaotong University for providing the thermal engineering laboratory for this research and all the laboratory teachers for their hard work.

Conflicts of Interest: The authors declare no conflict of interest.

Nomenclature

Symbol	Description
V	max element size, mm^3
ρ	Air density, kg/m^3
k	Turbulent kinetic energy, m^2/s^2

References

1. Kong, L.; Sun, S. The application of aluminum radiator on foreign locomotives. *Railw. Locomot. Mot. Car.* **2011**, *3*, 1–5.
2. Li, W.; Yu, Z. Heat exchangers for cooling supercritical carbon dioxide and heat transfer enhancement: A review and assessment. *Energy Rep.* **2021**, *105*, 4085–4105. [CrossRef]
3. Muhammad, A.; Arafat, A.B. Heat and mass transfer for compact heat exchanger (CHXs) design: A state-of-the-art review. *Int. J. Heat Mass Transf.* **2018**, *563*, 359–380.
4. Máté, P.; Gábor, S.; Károly, J. CFD analysis and heat transfer characteristics of finned tube heat exchangers. *Pollack Period.* **2019**, *32*, 156–168.
5. Kim, D.Y.; Cheon, H. A CFD-based design optimization of air-cooled passive decay heat removal system. *Nucl. Eng. Des.* **2018**, *102*, 351–363. [CrossRef]
6. Aris, M.S.; McGlen, R.; Owen, I.; Sutcliffe, C.J. An experimental investigation into the deployment of 3-D, finned wing and shape memory alloy vortex generators in a forced air convection heat pipe fin stack. *Appl. Therm. Eng.* **2011**, *31*, 1086–1100. [CrossRef]
7. Haider, P.; Freko, P.; Acher, T.; Rehfeldt, S.; Klein, H. Influence of inlet configuration and distributor geometry on the performance of cryogenic plate-fin heat exchangers. *Appl. Therm. Eng.* **2021**, *120*, 902–915. [CrossRef]
8. Gu, Y.; Liao, Q.; Ding, Y.; Cheng, M.; Wang, H.; Zhu, X. Experimental study of moist air condensation outside three-dimensional finned tubes with different fin parameters. *Int. J. Heat Mass Transf.* **2021**, *102*, 501–516. [CrossRef]
9. Dzierzgowski, M. Verification and improving the heat transfer model in radiators in the wide change operating parameters. *Energies* **2021**, *14*, 6543. [CrossRef]
10. Sebastian, U.; Matthias, B.; Samira, G.; Robin, W.; Uwe, H. Experimental study on the air-side thermal-flow performance of additively manufactured heat exchangers with novel fin designs. *Int. J. Therm. Sci.* **2019**, *85*, 305–319.
11. Effendi, N.S.; Byoung, G.K.; Jeong, S.P.; Kyoung, J.K. Fin spacing effects on the heat transfer performances of hollow hybrid fin heat sinks under air impingement. *J. Mech. Sci. Technol.* **2019**, *182*, 175–177.
12. Abhishek, P.; Prabha, C. Experimental investigations on thermal performance of solar air heater with wavy fin absorbers. *Heat Mass Transf.* **2019**, *65*, 2651–2666.
13. Zullo, F.; Giorgi, C. On the optimal shape and efficiency improvement of fin heat sinks. *Energies* **2023**, *16*, 316. [CrossRef]
14. Rajesh, B.C.; Kumar, P.; Roy, S.; Kanungo, D. CFD analysis of an economizer for heat transfer enhancement using serrated finned tube equipped with variable fin segments. *Mater. Today Proc.* **2020**, *45*, 1632–1644. [CrossRef]
15. Pungaiah, S.S.; Kailasanathan, C.K. Thermal analysis and optimization of nano coated radiator tubes using computational fluid dynamics and taguchi method. *Coatings* **2020**, *10*, 804. [CrossRef]
16. Deepika, K.; Sarviya, R.M. Application based review on enhancement of heat transfer in heat exchangers tubes using inserts. *Mater. Today Proc.* **2021**, *44*, 2362–2365. [CrossRef]
17. Le, X.H.K.; Pop, I.; Sheremet, M.A. Thermogravitational convective flow and energy transport in an electronic cabinet with a heat-generating element and solid/porous finned heat sink. *Mathematics* **2022**, *10*, 34. [CrossRef]
18. Chen, H.T.; Chang, Y.L.; Lin, P.Y.; Chiu, Y.J.; Chang, J.R. Numerical study of mixed convection heat transfer for vertical annular finned tube heat exchanger with experimental data and different tube diameters. *Int. J. Heat Mass Transf.* **2018**, *22*, 931–947. [CrossRef]
19. Dawid, T.; Jan, T.; Marcin, T. Experimental verification of an analytical mathematical model of a round or oval tube two-row car radiator. *Energies* **2020**, *13*, 3399.
20. Chikurde, R.C.; Kothavale, B.S.; Sane, N.K. Numerical validation of natural convection heat transfer with horizontal rectangular fin array using straight knurling patterns on fins—Correlation for Nusselt number. *Heat Transf. Asian Res.* **2019**, *12*, 1622–1647. [CrossRef]
21. René, H.; Hannes, V.; Leopold, P. Optimized heat exchanger integration within a TSA-process based on experimentally evaluated heat transfer correlations for finned-tubes in fluidized-beds. *Powder Technol.* **2019**, *356*, 957–973.
22. Malavasi, M.; Cattani, L.; Vocale, P.; Bozzoli, F.; Rainieri, S. Thermal characterisation of triple tube heat exchangers by parameter estimation approach. *Int. J. Heat Mass Transf.* **2021**, *8*, 1001–1016. [CrossRef]
23. Bošnjaković, M.; Čikić, A.; Muhič, S.; Holik, M. Heat transfer correlations for star-shaped fins. *Appl. Sci.* **2021**, *25*, 5912. [CrossRef]
24. Bisri, H.; Wijayanto, D.S.; Ranto. Effect of biodiesel and radiator tube heater on fuel consumption of compression ignition engine. *IOP Conf. Ser. Mater. Sci. Eng.* **2018**, *288*, 756–768. [CrossRef]
25. Kasper, L.; Pernsteiner, D.; Koller, M.; Schirrer, A.; Jakubek, S.; Hofmann, R. Numerical studies on the influence of natural convection under inclination on optimal aluminium proportions and fin spacings in a rectangular aluminium finned latent-heat thermal energy storage. *Appl. Therm. Eng.* **2020**, *22*, 150–165. [CrossRef]
26. Yu, C.; Xue, X.Y.; Shi, K.; Shao, M.Z.; Liu, Y. Comparative study on CFD turbulence models for the flow field in air cooled radiator. *Processes* **2020**, *8*, 1687. [CrossRef]
27. Savino, S.; Nonino, C. Header shape effect on the inlet velocity distribution in cross-flow double-layered microchannel heat sinks. *Fluids* **2022**, *7*, 7. [CrossRef]
28. Wijayanto, D.S.; Pambudi, N.A.; Wijaya, Y.; Rohman, N.; Bugis, H. Biodiesel fuel blend performance evaluation using a radial finned tube heater. *World J. Eng.* **2018**, *15*, 1122–1135. [CrossRef]
29. Wang, B.; Feng, S.; Liu, J.; Jiang, Y.K. Analysis of the signal-to-noise ratio of the cold-side fins of the airfoil tube radiator for construction vehicles. *J. Eng. Thermophys.* **2018**, *39*, 1849–1857.
30. Sebastian, U.; Matthias, B.; Johanna, T.; Uwe, H. Experimental study of the natural convection heat transfer performance for finned oval tubes at different tube tilt angles. *Exp. Therm. Fluid Sci.* **2019**, *55*, 100–108.

31. Haghighi, S.S.; Goshayeshi, H.R.; Safaei, M.R. Natural convection heat transfer enhancement in new designs of plate-fin based heat sinks. *Int. J. Heat Mass Transf.* **2018**, *26*, 640–647. [CrossRef]
32. Gragnaniello, L.; Iasiello, M.; Mauro, G.M. Multi-Objective optimization of a heat sink for the thermal management of a peltier-cell-based biomedical refrigerator. *Energies* **2022**, *15*, 7352. [CrossRef]
33. Talebi, M.; Lalgani, F. Assessment of thermal behavior of variable step twist in the elliptical spiral tube heat exchanger. *Int. J. Therm. Sci.* **2021**, *8*, 100–108. [CrossRef]
34. Cheng, L.; Liu, J.; Wang, B.; Qian, X.; Wang, X. The influence of airfoil fins on the heat dissipation performance of tube fin radiator. *Sci. Technol. Eng.* **2020**, *20*, 1163–1170.
35. Maisuria, M.B.; Sonar, D.M.; Rathod, M.K.; Bhatt, M.K. Experimental and analytical investigation on an automobile radiator with CuO/EG-water based nanofluid as coolant. *Heat Transf. Asian Res.* **2019**, *48*, 160–176. [CrossRef]
36. Mohammad, S.D.; Hassan, H. Numerical study on performance enhancement of the fin and tube heat exchanger using different nanoparticle shapes. *Int. J. Environ. Sci. Technol.* **2021**, *12*, 1–16.
37. Nóbrega, C.S.; Kamal, A.R.; Lino, F. Thermal performance of bare and finned tubes submersed in nano-PCM mixture. *J. Braz. Soc. Mech. Sci. Eng.* **2021**, *6*, 105–117. [CrossRef]
38. Nguyen, D.H.; Ahn, H.S. A comprehensive review on micro/nanoscale surface modification techniques for heat transfer enhancement in heat exchanger. *Int. J. Heat Mass Transf.* **2021**, *25*, 1100–1117. [CrossRef]
39. Faridi, K.R.; Ghafouri, A.; Halalizade, M. Numerical study of the effects of geometric parameters and nanofluid properties on heat transfer and pressure drop in helical tubes. *SN Appl. Sci.* **2021**, *16*, 1805–1819.
40. Jin, R.; Yang, X.; Yang, L.; Du, X.; Yang, Y. Thermo-flow performances of air-cooled condenser cell with oblique finned tube bundles. *Int. J. Therm. Sci.* **2019**, *135*, 1002–1017. [CrossRef]
41. Wadhah, H.; Doori, A. Numerical estimation of pressure drop and heat transfer characteristics in annular-finned channel heat exchangers with different channel configurations. *Heat Transf. Asian Res.* **2019**, *22*, 1280–1291.
42. Muhammad, A.; Hassan, A.; Shahid, I.; Sajid, K.; Farukh, F. Effect of condensate flow rate on retention angle on horizontal low-finned tubes. *Therm. Sci. J.* **2018**, *12*, 435–441.
43. Gülay, Y. Experimental investigation of forced convection heat transfer over horizontal tube with conical fins for different fin spacings and different inclination angles. *Trans. Can. Soc. Mech. Eng.* **2018**, *56*, 427–435.
44. Promvonge, P.; Skullong, S. Enhanced heat transfer in rectangular duct with punched winglets. *Chin. J. Chem. Eng.* **2020**, *28*, 130–148. [CrossRef]
45. Shubham, V.; Harishchandra, T. Comparison of natural convection heat transfer from a vertical cylinder fitted with annular step fins and annular triangular fins. *Int. J. Veh. Struct. Syst.* **2018**, *22*, 363–366.
46. Li, J. *Research on Numerical Simulation and Structure Optimization of Tube-Fin Double-Channel Radiator*; Dalian Jiaotong University: Dalian, China, 2017.
47. Ankur, K.; Jyeshtharaj, B.J.; Arun, K.N. A comparison of thermal-hydraulic performance of various fin patterns using 3D CFD simulations. *Int. J. Heat Mass Transf.* **2017**, *56*, 336–356.
48. Fang, J.; Yin, X.; Wang, A.; Sun, X.; Liu, Y.; Cao, F. Cooling performance enhancement for the automobile transcritical CO_2 air conditioning system with various internal heat exchanger effectiveness. *Appl. Therm. Eng.* **2021**, *196*, 117274. [CrossRef]
49. Guan, X.; Xie, Z.; Nan, G.; Xi, K.; Lu, Z.; Ge, Y. Thermal–Hydrodynamic behavior and design of a microchannel pin-fin hybrid heat sink. *Micromachines* **2022**, *13*, 2136. [CrossRef]
50. Wang, Y.; Zhang, J.; Zhang, Y.; Geng, L. *ANSYS Icepak*; Publishing House of Electronics Industry: Beijing, China, 2021; pp. 302–331.
51. Menon, S.H.; Rao, A.R.; Mathew, J.; Jayaprakash, J. Derivation of navier-stokes equation in rotational frame for engineering flow analysis. *Int. J. Thermofluids* **2021**, *11*, 100096. [CrossRef]
52. Chaoqun, L. New ideas on governing equations of fluid dynamics. *J. Hydrodyn.* **2021**, *6*, 1–6.
53. Javier, A.; Gabriel, N.G.; Ricardo, O. A posteriori error analysis of a mixed-primal finite element method for the boussinesq problem with temperature-dependent viscosity. *J. Sci. Comput.* **2019**, *10*, 887–917.
54. Said, M.; Hassan, E.G. On some initial and initial boundary value problems for linear and nonlinear boussinesq models. *Symmetry* **2019**, *20*, 1273.
55. Deng, X.; Li, E.; Wang, H. A variable-fidelity multi-objective evolutionary method for polygonal pin fin heat sink design. *Sustainability* **2023**, *15*, 1104. [CrossRef]
56. Han, Z.; Guo, J.; Zhang, H.; Chen, J.; Huai, X.; Cui, X. Experimental and numerical studies on novel airfoil fins heat exchanger in flue gas heat recovery system. *Appl. Therm. Eng.* **2021**, *6*, 850–865. [CrossRef]
57. Qiu, S.; Xu, C.; Yang, Z.; He, H.; Xia, E.; Xue, Z.; Li, L. One-dimension and three-dimension collaborative simulation study of the influence of non-uniform inlet airflow on the heat transfer performance of automobile radiators. *Appl. Therm. Eng.* **2021**, *10*, 1225–1238. [CrossRef]
58. Li, F.; Zhu, W.; He, H. Numerical optimization on microchannel flow and heat transfer performance based on field synergy principle. *Int. J. Heat Mass Transf.* **2019**, *20*, 375–385. [CrossRef]